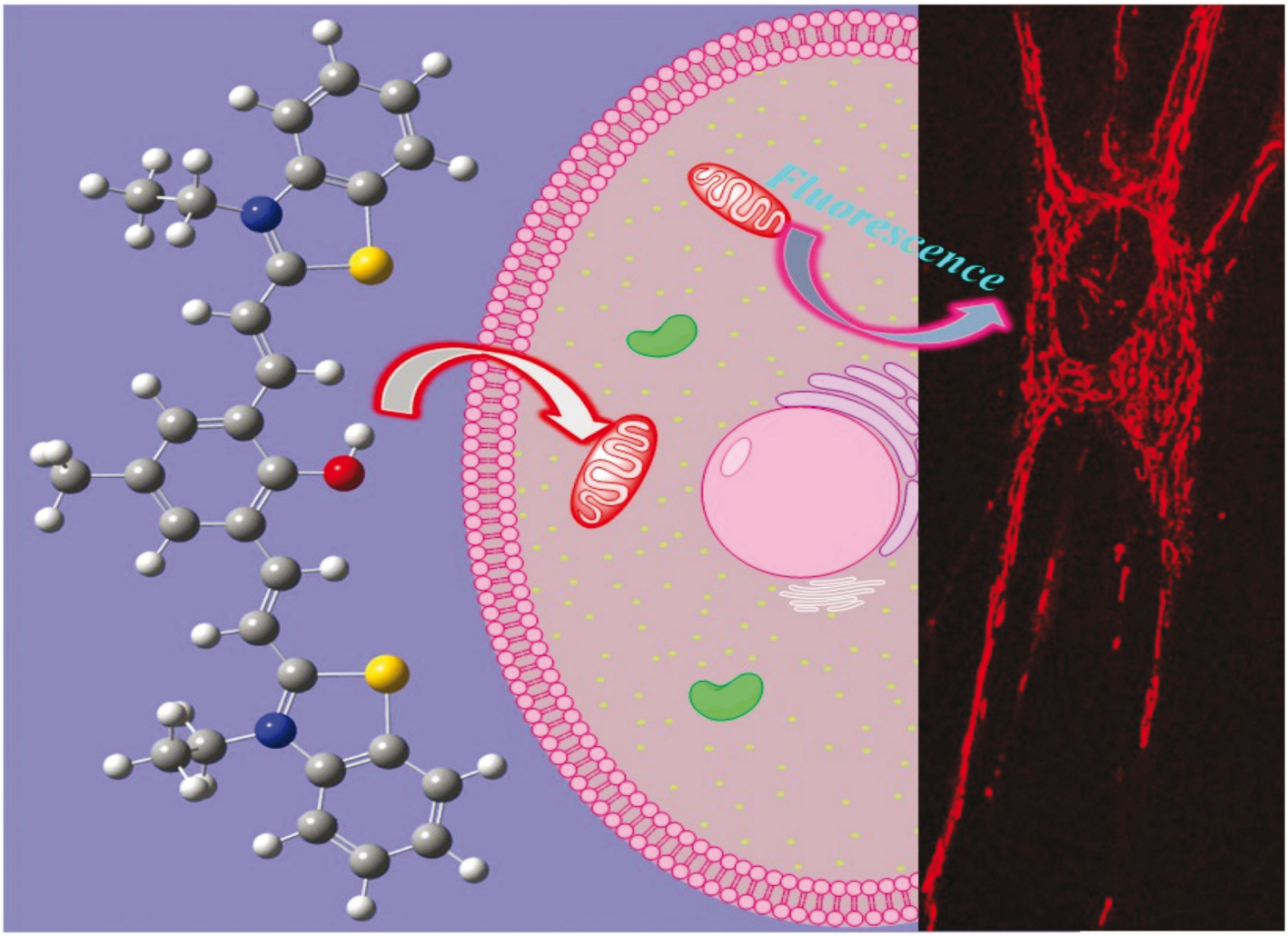

Showcasing research from Professor Yi Pang's laboratory, Department of Chemistry, University of Akron, Akron, Ohio, USA.

A NIR-emitting cyanine with large Stokes shifts for live cell imaging: large impact of the phenol group on emission

There are a limited number of near-infrared (NIR) emitting molecular probes available for imaging applications. A fluorescent cyanine with NIR emission ($\lambda_{em} \approx 800$ nm) and large Stokes shift was found to exhibit excellent selectivity towards mitochondria for live-cell imaging.

As featured in:

See Yi Pang *et al.*, *Chem. Commun.*, 2019, **55**, 13223.

ROYAL SOCIETY OF CHEMISTRY | Celebrating IYPT 2019

rsc.li/chemcomm

Registered charity number: 207890

ChemComm

COMMUNICATION

View Article Online
View Journal | View Issue

Cite this: *Chem. Commun.*, 2019, **55**, 13223

Received 2nd September 2019,
Accepted 26th September 2019

DOI: 10.1039/c9cc06831g

rsc.li/chemcomm

A NIR-emitting cyanine with large Stokes shifts for live cell imaging: large impact of the phenol group on emission†

Dipendra Dahal, Lucas McDonald, Sabita Pokhrel, Sailaja Paruchuri, Michael Konopka and Yi Pang *

There are a limited number of near-infrared (NIR) emitting (λ_{em} = 700–900 nm) molecular probes for imaging applications. A NIR-emitting probe that exhibits emission at ~800 nm with a large Stokes shift was synthesized and found to exhibit excellent selectivity towards mitochondria for live-cell imaging. The photophysical properties were attributed to an excited "cyanine structure" *via* intramolecular charge transfer (ICT) involving a phenol group.

Visualization of specific organelles and organs by fluorescent agents has been the center of recent research because of their high sensitivity, low cost, and high specificity.[1–3] The applications depend on the probe's ability to target the specific organelles (or organs) without perturbation of their morphology and physiology. For example, mitochondria are double layer membrane-bound organelles which exist in eukaryotic cells and are responsible for the generation of the entire cellular energy in an animal cell in the form of ATP.[4–7] The function of mitochondria is dependent on the electrochemical gradient potential ($\Delta\psi_m$) across mitochondrial membranes or electrochemical proton motive force (Δp), which is a combination of mitochondrial membrane potential and mitochondrial pH gradient generated by a respiratory electron transport chain (ETC).[4,7–9] Damage and dysfunction of mitochondria are associated with various diseases including aging, cancer, neurodegenerative diseases, Alzheimer's disease, Huntington disease, diabetes, and Parkinson's disease.[7,10–12]

Most of the fluorescent probes absorb and emit in the visible region, and their application is limited by high phototoxicity and interference from background fluorescence.[13] NIR-emitting fluorescent probes[14] are useful for bioimaging applications, as they suffer less auto-fluorescence from the biological samples and can achieve deeper tissue penetration.[15] Current NIR-emitting probes include BODIPY, benzofuran, rhodamine, and cyanine as fluorophores.[16,17] However, these fluorophores have small Stokes shifts ($\Delta\lambda \approx$ 10–60 nm), which prevent the optimum collection of fluorescence signals and hamper their broad applications in bioimaging.[18–20] Therefore, developing fluorophores with large Stokes shifts is desirable, in order to realize the full potential of sensitive fluorescence imaging. In addition, NIR-emitting fluorescent probes with significant Stokes shifts are also useful for single excitation multicolor live-cell imaging, which plays an important role in biological studies.[21]

Recently, our group synthesized NIR emitting probe **1** (Fig. 1), which gives NIR emission with very large Stokes shifts ($\Delta\lambda \approx$ 234 nm).[22,23] The molecular structure of **1** integrates an "excited state intramolecular proton transfer (ESIPT)" group with a hemicyanine unit *via* sharing a *meta*-phenylene bridge. Interestingly, probe **1** exhibits excellent selectivity toward intracellular lysosomes, due to the low pK_a (= 5.72) of its phenolic

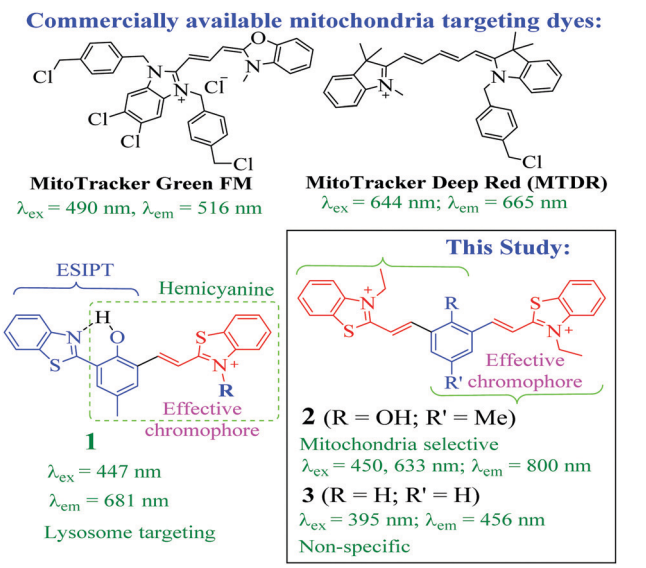

Fig. 1 Chemical structures of probes **1–3** and some commercial mitochondria staining dyes.

Department of Chemistry, The University of Akron, Akron, OH 44325, USA. E-mail: yp5@uakron.edu

† Electronic supplementary information (ESI) available: Synthesis and characterization of **2** and **3**; ^{1}H NMR and mass spectral data; and additional UV-vis absorption and fluorescence data. See DOI: 10.1039/c9cc06831g

proton and its ability to give a large fluorescence turn on in an acidic environment ($ArO^- + H^+ \rightarrow ArOH$).[22] It should be noted that the effective chromophores in **1** can be approximated by hemicyanine and ESIPT fragments, due to π-conjugation interruption by a *meta*-phenylene bridge.[24] In an effort to further examine the structural impact on the fluorescence properties, herein, we illustrate the synthesis of **2**, in which the effective chromophore is nearly the same as that in **1**. In probe **2**, the phenolic proton can dissociate but does not undergo any intramolecular proton transfer reaction. Interestingly, probe **2** exhibits NIR emission ($\lambda_{em} \approx 800$ nm) with a very large Stokes shift (*e.g.* $\Delta\lambda \approx 161$ nm), in sharp contrast to conventional cyanine dyes ($\Delta\lambda \approx 10$–60 nm). Although the phenolic proton of **2** is acidic ($pK_a \approx 4$), probe **2** exhibits remarkable selectivity toward mitochondria when used to stain biological cells.

The desired compound **2** was synthesized by the reaction of 2-hydroxy-5-methylisophthalaldehyde (dialdehyde) with 1-ethyl-2-methylbenzothiazolium salt in 75% yield (see ESI† for detail) and was characterized by NMR and mass spectrometry. The ^{1}H NMR spectrum of **2** gave sharp doublet signals at 8.0 and 8.4 ppm, which were attributed to newly formed vinyl bonds (Fig. 2). The high-resolution mass spectrum revealed *m/z* 483.1119 that was the deprotonated state of **2** without counter ions (Fig. S4, ESI†); calcd for 483.1553. Compound **3** (*m/z* 454.1500, ESI,† Fig. S7; calcd for 454.1526) was also synthesized to aid the spectral study.

The UV-vis absorption spectra of **2** revealed the absorption peaks at $\lambda_{abs} \approx 395$ and a broad shoulder at 456 nm, similar to that observed for **1** due to the presence of identical effective chromophores in **1** and **2**.[22] However, a new absorption peak at $\lambda_{max} \approx 717$ nm was observed for **2**. The absorption bands at $\lambda_{abs} \approx 395$ and 456 nm were attributed to the enol form (or acid form) **2a**, while the band at 717 nm was attributed to its base form **2b** (Scheme 1). Since only one set of resonance signals (*e.g.* for H_b and H_c) was observed in the ^{1}H NMR spectrum, compound **2** was assumed to be present predominantly in its enol form **2a** in a polar aprotic solvent.

Interestingly, the emission of **2** showed $\lambda_{em} \approx 784$ nm (Fig. 3 and Table 1). The results indicated a strong synergistic interaction between the two hemicyanine substituents in **2**, since the λ_{em} value of **2** was significantly red-shifted from that of **1** ($\lambda_{em} \approx 681$ nm).[22] The observed spectral red-shift was apparently dependent on the presence of the –OH group between the

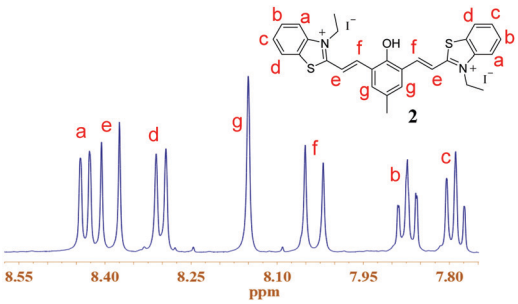

Fig. 2 ^{1}H NMR spectrum of **2** in DMSO-d_6, showing the resonance signals of aromatic protons (the alkyl region is omitted for clarity).

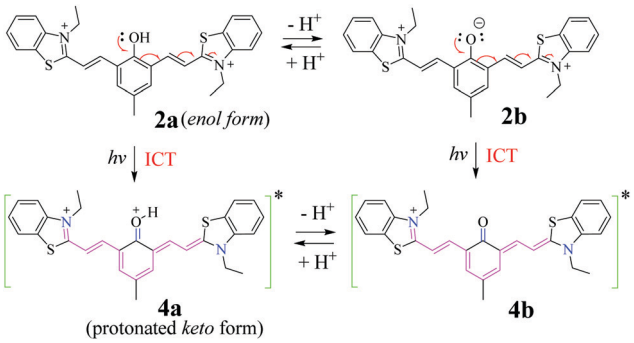

Scheme 1 The proposed transformation of excited **2** to its keto form **4**, and their equilibrium *via* proton dissociation.

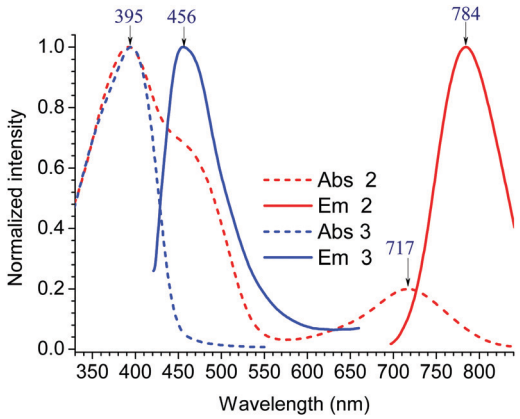

Fig. 3 UV-vis absorption (broken line) and emission spectra (solid line) of **2** and **3** in CH_2Cl_2. The excitation wavelengths were 687 nm for **2** and 395 nm for **3**.

substituents, as the NIR emission band was not observed for the model compound **3** (λ_{abs} = 395 nm and λ_{em} = 456 nm; Fig. S12 and S13, ESI†).

Examination of **2** in different solvents revealed that its NIR absorption peak was affected by solvent polarity (λ_{abs} = 728 nm in DMSO, but 589 nm in aqueous solution) (Table 1 and Fig. S8, ESI†). However, the emission wavelength of **2** was less affected (λ_{em} = 770–804 nm) (Fig. S9, ESI†). DFT calculations with the TD-SCF method revealed that the keto tautomer of **2** in CH_2Cl_2 showed absorption (λ_{abs} = 714 nm) and emission (λ_{em} = 780 nm) (Fig. S10, ESI†), which closely matched the experimental values (λ_{abs} = 717 nm and λ_{em} = 784 nm).

Table 1 Photophysical properties of compounds **2** and **3** in different solvents

	Compound 2			Compound 3		
Solvents	λ_{abs}	λ_{em}	(Φ_{fl})	λ_{abs}	λ_{em}	(Φ_{fl})
DCM	392, 456, 717	784	0.11	395	456	0.004
DMF	388, 489, 728	803	0.04	383	470	0.002
DMSO	388, 728	803	0.04	387	467	0.002
EtOH	385, 654	798	0.03	384	460	0.002
MeCN	382, 702	795	0.04	382	460	0.002
MeOH	382, 633	794	0.02	383	460	0.002
Water	382, 589	770	0.01	380	460	0.002

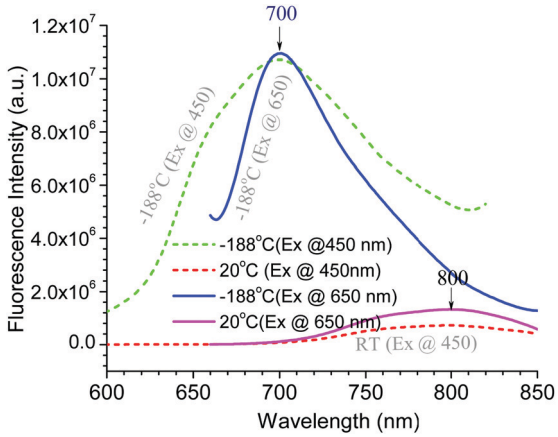

Fig. 4 Fluorescence spectra of **2** at room temperature and low temperature, with λ_{ex} of 450 nm (dotted lines) and 650 nm (solid lines).

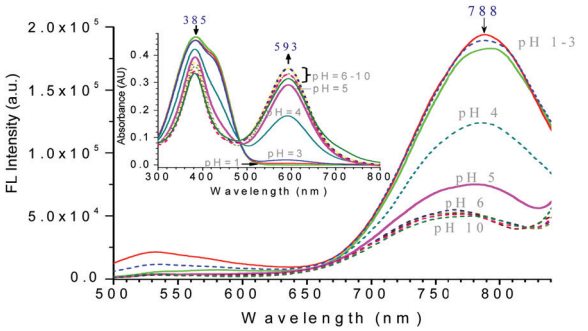

Fig. 5 Fluorescence spectra of **2** (10 μM) in different pH buffers in water (excitation at 448 nm). The inset shows the UV-absorption of the corresponding solution.

The observed NIR emission from **2** could be attributed to the formation of its keto form **4** (Scheme 1). Traditionally, one would assume that **4b** is the species responsible for the NIR emission. An interesting question is where the protonated keto form **4a** would give emission. In order to shed some light on their emissive properties, we decided to freeze the dilute solution of **2** by liquid nitrogen, which would eliminate the dynamic impact of chemical equilibrium between **2a** and **2b**. Thus, a solution of **2** (in EtOH) in a quartz tube was cooled by immersing it into liquid nitrogen in a quartz Dewar, and the fluorescence emission spectra were acquired by exciting the sample at 450 nm (Fig. S14, ESI†) and 650 nm (Fig. S15, ESI†) at different temperatures. At low temperature (at −189 °C), emission of **2** became more intense and blue-shifted to $\lambda_{em} \approx$ 700 nm (Fig. 4), as the probe molecules were frozen in a rigid solvent matrix (EtOH m.p. = −112 °C). However, when the enol form **2a** was excited selectively at 450 nm, the emission spectra revealed only one peak that had similar λ_{em} when the sample was excited at 650 nm (λ_{ex} for keto form **2b**). The result indicated that the enol form **2a** also gave NIR emission.

The pH response of **2** was examined by acquiring the optical spectra in different pH buffer solutions in water. In strongly acidic buffer pH = 1–3, **2** exhibited only one absorption band at 385 nm (Fig. 5 and Fig. S17, ESI†), indicating that the equilibrium was completely shifted to **2a** (Scheme 1). As pH increased, an additional absorption peak was observed at ~593 nm, which could be attributed to the deprotonation of the phenolic proton. The pK_a of **2** was determined to be 4.0 by the Boltzmann fitting (Fig. S18, ESI†), showing that the phenolic proton was quite acidic as a consequence of two electron-withdrawing benzothiazolium groups. Interestingly, the fluorescence of **2** revealed only one major emission peak at $\lambda_{em} \approx$ 788 nm in the entire pH range examined. When pH = 1–3, probe **2** was expected to be in the enol form **2a**, as revealed from its UV-vis spectra. Upon excitation, **2a** could undergo the intramolecular charge transfer (ICT), which led to its keto tautomer **4a** (Scheme 1). A notable feature was that the keto form **4a** was only formed in the excited state, giving the fluorescence at $\lambda_{em} \approx$ 788 nm with a very large Stokes shift.

It should be notable that there was a significant difference between the optical properties of **1** and **2**. Under alkaline conditions (*e.g.*, pH = 9–11), the resulting phenoxide from **1** was non-fluorescent as ESIPT was no longer operative.[22] However, the phenoxide anion of **2** was still fluorescent, although the fluorescence intensity was higher at acidic pH (Fig. 5). Since the phenolic proton of **2** was quite acidic, the formation of the phenoxide anion at physiological pH allowed the excitation of **2** at a longer wavelength, thereby raising the prospect for bioimaging applications. Evaluation of **2** also revealed that the probe was insensitive to different anions such as acetate (ACO^-), adenosine monophosphate (AMP), adenosine diphosphate (ADP), adenosine triphosphate (ATP), pyrophosphate (PPi), biphosphate (HPO_4^{2-}), thiosulfate ($S_2O_3^{2-}$), perchlorate (ClO_4^-), bisulfite (HSO_3^-), fluoride (F^-), hydrogen peroxide (H_2O_2) and some biothiols like cysteine (Cys), glutathione (GSH), and bovine serum albumin (BSA) (Fig. S19a and S20a, ESI†). Considering the high abundance of glutathione in cells, compound **2** was treated with very high concentration of GSH (up to 10 mM), the optical properties of compound **2** were not affected by the use of 1 mM (50 equivalents) of GSH. However, absorbance was blue shifted (Fig. S19b, ESI†) and emission intensity decreased (Fig. S20b, ESI†) with the addition of 5 mM (250 equivalents) concentration of GSH.

The fluorescence properties of **2** encouraged us to seek their potential applications for bioimaging. Cell viability studies by performing MTT assay showed the half-maximal cell inhibitory concentration (IC50) of 24.72 μM for **2** (Fig. S21, ESI†), indicating its low toxicity. When using **2** to stain normal human lung fibroblast (NHLF) cells, confocal microscopy imaging (Fig. 6B and Fig. S22, ESI†) displayed fluorescence signals in a non-uniform pattern, indicating that the dye might bind to intracellular organelles selectively. Co-staining of **2** with MitoTracker Green FM showed good colocalization (Fig. 6C). The results confirmed that **2** exhibited excellent selectivity to the mitochondria, with a Pearson's correlation coefficient 0.79 (Fig. 6C and F). The results indicated that **2** was selective toward mitochondrial organelles, despite the fact that the probe would give higher fluorescence in an acidic environment (pK_a = 4.01, and Fig. 5).

Probe **2** could be considered as a "functional mitochondrial probe" which is accumulated into mitochondria due to the potential gradient ($\Delta\psi_m$) of the mitochondrial matrix, as suggested

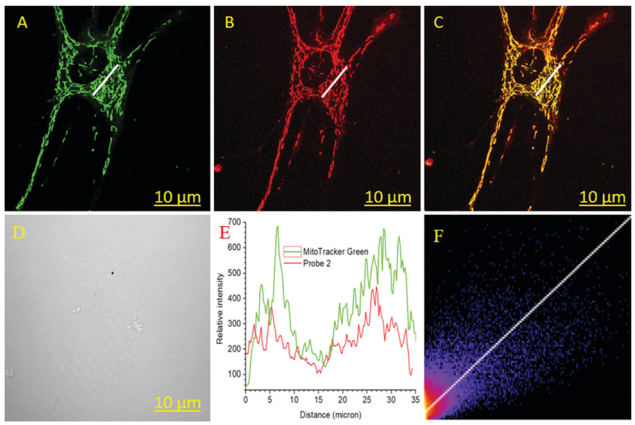

Fig. 6 Normal human lung fibroblast (NHLF) cells co-stained with **2** (1 μM) and MitoTracker green (200 nM), viewed in green (A) and NIR channel (B), merged A and B (C) and bright field (D). (E) The plot of relative intensity *vs.* distance for probe **2** and MitoTracker Green for the region in the white line in (A) and (B), and (F) correlation plot between MitoTracker Green and **2**. Excitation/emission $\lambda_{ex}/\lambda_{em}$ = 488/525 nm for MitoTracker Green, and 640/(680–735) nm for **2**.

by using **2** in fixed cells (Fig. S24, ESI†). Compound **2** was also treated in different cell lines of human oligodendrocytes (MO.3.13 cells, Fig. S23, ESI†), the colocalization of **2** with MitoTracker Green demonstrated that there was proper overlapping between MitoTracker Green and compound **2** with a Pearson's correlation coefficient of 0.67 which indicated that probe **2** was selective to mitochondrial organelles in the live oligodendrocyte cells. It should be noted that fluorescence imaging was acquired with a 680–735 nm emission filter (due to the availability), and brighter imaging could be observed if the emission filter was near the peak fluorescence at ~788 nm. The results pointed that **2** could be a useful molecular probe for bioimaging.

In summary, NIR ($\lambda_{em} \approx 800$ nm) emitting probe **2** was synthesized, which showed large Stokes shifts *via* the ICT mechanism. Probe **2** possessed an acidic phenol group with pK_a = 4.01, which allowed the formation of the keto-form to facilitate ICT interaction in the excited state. This extended the conjugation, thereby shifting the absorption and emission to the NIR region. The acidic phenol group in the *meta*-phenylene bridge plays a vital role in the optical properties of **2**, as compound **3** without the phenol group gave weak emission at a much shorter wavelength ($\lambda_{em} \approx 470$). Probe **2** with double positive charges was assumed to play a decisive role in the observed mitochondrial selectivity, due to Coulombic attraction toward the negative potential gradient of the mitochondrial matrix. Low cytotoxicity of **2** and its attractive NIR emission suggest that the probe could have promising application in live-cell imaging.

We acknowledge support from NIH (Grant No. 1R15GM126438-01A1) and partial support from Coleman Endowment from The University of Akron. We thank Savannah Snyder for acquiring mass spectrometric data.

Conflicts of interest

There are no conflicts to declare.

References

1 T. Nagaya, Y. A. Nakamura, P. L. Choyke and H. Kobayashi, *Front. Oncol.*, 2017, **7**, 314.
2 M. Grossi, M. Morgunova, S. Cheung, D. Scholz, E. Conroy, M. Terrile, A. Panarella, J. C. Simpson, W. M. Gallagher and D. F. O'Shea, *Nat. Commun.*, 2016, **7**, 10855.
3 A. C. Sedgwick, L. Wu, H.-H. Han, S. D. Bull, X.-P. He, T. D. James, J. L. Sessler, B. Z. Tang, H. Tian and J. Yoon, *Chem. Soc. Rev.*, 2018, **47**, 8842–8880.
4 N. Zhao, S. Chen, Y. Hong and B. Z. Tang, *Chem. Commun.*, 2015, **51**, 13599–13602.
5 S. Gandre-Babbe and A. M. van der Bliek, *Mol. Biol. Cell*, 2008, **19**, 2402–2412.
6 J. R. Friedman and J. Nunnari, *Nature*, 2014, **505**, 335.
7 Z. Xu and L. Xu, *Chem. Commun.*, 2016, **52**, 1094–1119.
8 E. Gottlieb, S. M. Armour, M. H. Harris and C. B. Thompson, *Cell Death Differ.*, 2003, **10**, 709.
9 S. W. Perry, J. P. Norman, J. Barbieri, E. B. Brown and H. A. Gelbard, *Biotechniques*, 2011, **50**, 98–115.
10 Y. Liu, J. Zhou, L. Wang, X. Hu, X. Liu, M. Liu, Z. Cao, D. Shangguan and W. Tan, *J. Am. Chem. Soc.*, 2016, **138**, 12368–12374.
11 B. Liu, M. Shah, G. Zhang, Q. Liu and Y. Pang, *ACS Appl. Mater. Interfaces*, 2014, **6**, 21638–21644.
12 L. Long, M. Huang, N. Wang, Y. Wu, K. Wang, A. Gong, Z. Zhang and J. L. Sessler, *J. Am. Chem. Soc.*, 2018, **140**, 1870–1875.
13 K. Singh, A. M. Rotaru and A. A. Beharry, *ACS Chem. Biol.*, 2018, **13**, 1785–1798.
14 S. Wang, Y. Fan, D. Li, C. Sun, Z. Lei, L. Lu, T. Wang and F. Zhang, *Nat. Commun.*, 2019, **10**, 1058.
15 E. I. Altınoğlu, T. J. Russin, J. M. Kaiser, B. M. Barth, P. C. Eklund, M. Kester and J. H. Adair, *ACS Nano*, 2008, **2**, 2075–2084.
16 S. Zhang, T. Wu, J. Fan, Z. Li, N. Jiang, J. Wang, B. Dou, S. Sun, F. Song and X. Peng, *Org. Biomol. Chem.*, 2013, **11**, 555–558.
17 X. Zhang, Q. Sun, Z. Huang, L. Huang and Y. Xiao, *J. Mater. Chem. B*, 2019, **7**, 2749–2758.
18 W. Hu, H. Ma, B. Hou, H. Zhao, Y. Ji, R. Jiang, X. Hu, X. Lu, L. Zhang, Y. Tang, Q. Fan and W. Huang, *ACS Appl. Mater. Interfaces*, 2016, **8**, 12039–12047.
19 B. Wang, X. Cui, Z. Zhang, X. Chai, H. Ding, Q. Wu, Z. Guo and T. Wang, *Org. Biomol. Chem.*, 2016, **14**, 6720–6728.
20 W. Sun, S. Guo, C. Hu, J. Fan and X. Peng, *Chem. Rev.*, 2016, **116**, 7768–7817.
21 K. D. Piatkevich, B. P. English, V. N. Malashkevich, H. Xiao, S. C. Almo, R. H. Singer and V. V. Verkhusha, *Chem. Biol.*, 2014, **21**, 1402–1414.
22 D. Dahal, L. McDonald, X. Bi, C. Abeywickrama, F. Gombedza, M. Konopka, S. Paruchuri and Y. Pang, *Chem. Commun.*, 2017, **53**, 3697–3700.
23 Y. Guo, D. Dahal, Z. Kuang, X. Wang, H. Song, Q. Guo, Y. Pang and A. Xia, *AIP Adv.*, 2019, **9**, 015229.
24 Q. Chu, Y. Pang, L. Ding and F. E. Karasz, *Macromolecules*, 2003, **36**, 3848–3853.

